Environmental Science Advances

ROYAL SOCIETY OF CHEMISTRY

PAPER

View Article Online
View Journal | View Issue

Cite this: *Environ. Sci.: Adv.*, 2026, **5**, 1418

Spatiotemporal analysis of long-term air pollution in two urban regions of Vietnam and potential source contributions

Nguyen Thuy Huong,[a] Quang Tran Vuong,[b] Le Van Linh,[cd] Dam Duy An,[e] Van Huu Tap,[f] Nguyen Thi Pho,[a] Norimichi Takenaka[g] and Phan Quang Thang *[ad]

Air quality monitoring in Vietnam has been limited by sparse ground-based observations, leaving long-term pollution dynamics poorly understood. This study provides the first 43-year (1980–2023) spatiotemporal assessment of major pollutants including carbon monoxide (CO), sulfur dioxide (SO_2), black carbon (BC), and fine particulate matter ($PM_{2.5}$), across Vietnam's two largest urban–industrial regions. In addition, we combined remote sensing data, ground-based $PM_{2.5}$ data, statistical analyses, and source attribution modeling to disentangle local and transboundary influences on air quality in Vietnam. Overall, the concentrations of air pollutants were consistently 2–4 times higher in the North than in the South during the last five years (CO: 2.30; SO_2: 4.43; BC: 3.40, PM_{25}: 4.14 times). BC was strongly correlated to $PM_{2.5}$ (ρ up to 0.97, $p < 0.01$), demonstrating its central role in $PM_{2.5}$ composition. The Modern-Era Retrospective Analysis for Research and Applications, Version 2 (MERRA-2) reproduced seasonal $PM_{2.5}$ variability in Hanoi ($\rho = 0.64 \div 0.82$) but underestimated dry–wet contrasts in Ho Chi Minh City, emphasizing the need for enhanced ground-based monitoring. Results of potential source contribution function (PSCF) highlighted northern $PM_{2.5}$ hotspots associated with transport from neighboring countries, while southern hotspots were more diffuse and strongly influenced by traffic, industrial, and shipping emissions. Moderate Resolution Imaging Spectroradiometer (MODIS) fire data confirmed biomass burning in the Mekong subregion during March–April as a significant episodic contributor to northern $PM_{2.5}$. The findings of this study provide a robust baseline for emission trend evaluation, targeted mitigation, and cross-border pollution management, offering critical evidence to support Vietnam's net-zero emission strategies.

Received 17th October 2025
Accepted 8th April 2026

DOI: 10.1039/d5va00367a

rsc.li/esadvances

Environmental significance

Air pollution in rapidly developing countries like Vietnam remains poorly characterized due to limited long-term monitoring, hindering effective mitigation strategies. Understanding spatiotemporal dynamics and source contributions is critical for protecting public health and supporting climate commitments. This study provides the first 43-year integrated assessment of key pollutants across Vietnam's two major urban–industrial regions, combining reanalysis, ground observations, and source attribution. We reveal pronounced north–south disparities, identify black carbon as a dominant driver of $PM_{2.5}$, and demonstrate the significant role of transboundary transport and seasonal biomass burning. These findings highlight the need for region-specific control strategies and strengthened monitoring systems, offering robust scientific evidence to guide air quality management and support Vietnam's net-zero goals.

1. Introduction

The concentrations of atmospheric pollutants are influenced by a complex interplay of emission sources, atmospheric transport and mixing, physical and chemical transformations, and removal processes through deposition. Since the early 2000s, the increasing availability of satellite observations of trace gases and aerosols has driven numerous efforts to integrate these

[a]*Institute of Science and Technology for Energy and Environment (ISTEE), Vietnam Academy of Science and Technology (VAST), 18 Hoang Quoc Viet Street, Nghia Do Ward, Hanoi, Vietnam. E-mail: phanquanthang@istee.vast.vn*

[b]*Institute of Smart City and Management, College of Technology and Design, University of Economics Ho Chi Minh City, Ho Chi Minh City, Vietnam*

[c]*Water Resources Institute, 8 Phao Dai Lang Street, Lang Ward, Hanoi, Vietnam*

[d]*Graduate University of Science and Technology (GUST), Vietnam Academy of Science and Technology (VAST), 18 Hoang Quoc Viet Street, Nghia Do Ward, Hanoi, Vietnam*

[e]*Center for Calibration of Environmental and Chemical Equipment, 29-F, A10, Nam Trung Yên Urban Area, Yen Hoa Ward, Hanoi, Vietnam*

[f]*Center for Advanced Technology Development, Thai Nguyen University, Thai Nguyen 24000, Vietnam*

[g]*Division of Sustainable System Sciences, Graduate School of Sustainable System Sciences, Osaka Metropolitan University, 1-1 Gakuen-Cho, Nakaku, Sakai, Osaka 599-8531, Japan*

datasets into atmospheric chemical models using data assimilation techniques.1–3 Data assimilation provides an objective approach to combine observational data with model-based estimates (background values), in order to provide the most likely estimate of the system state.[4] When trace gases and aerosols are assimilated consistently over extended periods using a single modeling and assimilation framework, the resulting products, known as atmospheric composition reanalyses, offer physically consistent datasets that can reveal the drivers of observed trends and seasonal or interannual variability.[4] Among the most widely used reanalysis products is the Modern-Era Retrospective Analysis for Research and Applications, Version 2 (MERRA-2), which provides open-access, long-term, and diverse global datasets on pollutant concentrations and aerosol species. MERRA-2 has demonstrated reasonable accuracy in capturing the spatial distribution of $PM_{2.5}$ in regions such as the United States and Europe, though it often underestimates concentrations in other areas, including the Eastern Mediterranean,[5] Iran,[6] and India.[7,8] In Vietnam, MERRA-2 has been applied in a limited number of studies. For example, Lasko *et al.*, (2018) examined the relationship between biomass burning in northern Vietnam and Laos and air quality in Hanoi,[9] while Nguyen *et al.*, (2025) assessed aerosol trends related to $PM_{2.5}$ and evaluated the model's performance in the Northern Key Economic Region.[10] However, comprehensive studies using MERRA-2 to assess a broader range of pollutants, such as CO, SO_2, BC, and $PM_{2.5}$, across Vietnam remain scarce. Vietnam's air quality challenges are exacerbated by rapid urbanization and industrialization, with Hanoi (HN) and Ho Chi Minh City (HCM) experiencing annual $PM_{2.5}$ levels[11] often exceeding WHO guidelines by 5–10 times.[12]

In Vietnam, HN and HCM are the two largest metropolitan areas, each serving as the core of key national economic regions that include multiple neighboring provinces. These regions host a combination of long-established and rapidly expanding industrial zones. Such industrial parks, encompassing diverse manufacturing and processing sectors, are major potential sources of air pollutant emissions, placing considerable pressure on the densely populated local environment. Analyzing the long-term and seasonal trends, as well as the spatial distribution, of air pollutants is essential for evaluating their impacts on public health and quality of life, and for providing a scientific foundation for environmental policy-making. This need is amplified by Vietnam's commitment to achieving net-zero greenhouse gas emissions by 2050, set against a backdrop of continued rapid industrialization. Emission control initiatives are being implemented in accordance with the Paris Agreement[13] and the ASEAN Agreement on Transboundary Haze Pollution,[14] reflecting a recognition of regional air quality decline and its links to climate change. Air pollutant concentrations in Vietnam are influenced by a combination of factors, including local emission sources, regional meteorological conditions, and long-range transport of pollutants. For instance, Hybrid Single Particle Lagrangian Integrated Trajectory (HYSPLIT) trajectory analyses by Cohen *et al.*, (2010), Ly *et al.*, (2021), and Phung Ngoc *et al.*, (2021) demonstrated that elevated wintertime $PM_{2.5}$ levels in northern Vietnam are partly attributable to air masses transported from China. Similarly, Vuong *et al.*, (2023) applied potential source contribution function (PSCF) analysis to assess the influence of surrounding regions on PM levels in Hanoi from April to September 2018, while T. N. T. Nguyen *et al.*, (2023) conducted a PSCF-based source apportionment for Ho Chi Minh City during 2019–2020. Vuong *et al.*, (2025) concludes that $PM_{2.5}$ level in HCM over period of 2016–2020 were significantly lower than those in HN and wind patterns played an important role in $PM_{2.5}$ in both cities. However, few studies have simultaneously applied such analyses to both northern and southern Vietnam over extended time periods using both satellite and ground-based data, resulting in a significant gap in understanding the spatially and temporally integrated dynamics of air pollution across the country. This study aims to address these gaps by (1) analyzing long-term (1980–2023) spatial and temporal trends of CO, SO_2, BC, and $PM_{2.5}$; (2) evaluating seasonal correlations and model validation; and (3) identifying potential source areas using PSCF and fire data.

2. Data and methodology

2.1. Study area and scope

Fig. 1 provides a spatial overview of the two main study zones: the Northern Zone (NZ), the domain covers 105 °E–107 °E, 20.5 °N–22 °N, which includes HN and its neighboring provinces, and the Southern Zone (SZ), the domain covers 105.5 °E–107 °E, 10 °N–11 °N, which encompasses HCM and its adjacent provinces. The two central cities, HN and HCM, have very high population densities (>5.8 million people), representing the two largest urban and economic centers in the country. Surrounding areas such as Bac Ninh, Hai Phong, Binh Duong, and Dong Nai also have relatively high populations (3–5 million), especially in the SZ.

Industrial parks (IPs) are densely distributed in both study regions, mainly clustering around HN and HCM. Details of the industrial zones are provided in the appendix (Tables S1 and S2). The northern region showed a trend of developing newer IPs after 2019. Since this year, Vietnam entered a new phase of environmental governance and industrial development with stricter environmental impact assessment enforced by the Law on Environmental Protection 2020. In the south, new IP development is concentrated to the east of HCM (toward Binh Duong and Dong Nai), where infrastructure and transport are rapidly advancing (following the Southeastern Region's development plan). The overlapping distribution between densely populated areas and concentrated industrial zones is a clear indicator of significant local emission sources (*e.g.*, traffic and industrial activities) and a high risk of severe local air pollution.

In this study, we assess long-term air pollution trends using pollutant data from 1980 to 2023. We then focus on the most recent five years: 2019–2023. To evaluate seasonal variability, the Northern region is analyzed according to four meteorological seasons: DJF (December–January–February), MAM (March–April–May), JJA (June–July–August), and SON (September–October–November). In contrast, for the Southern region, the wet season extends from May to November, while the dry season

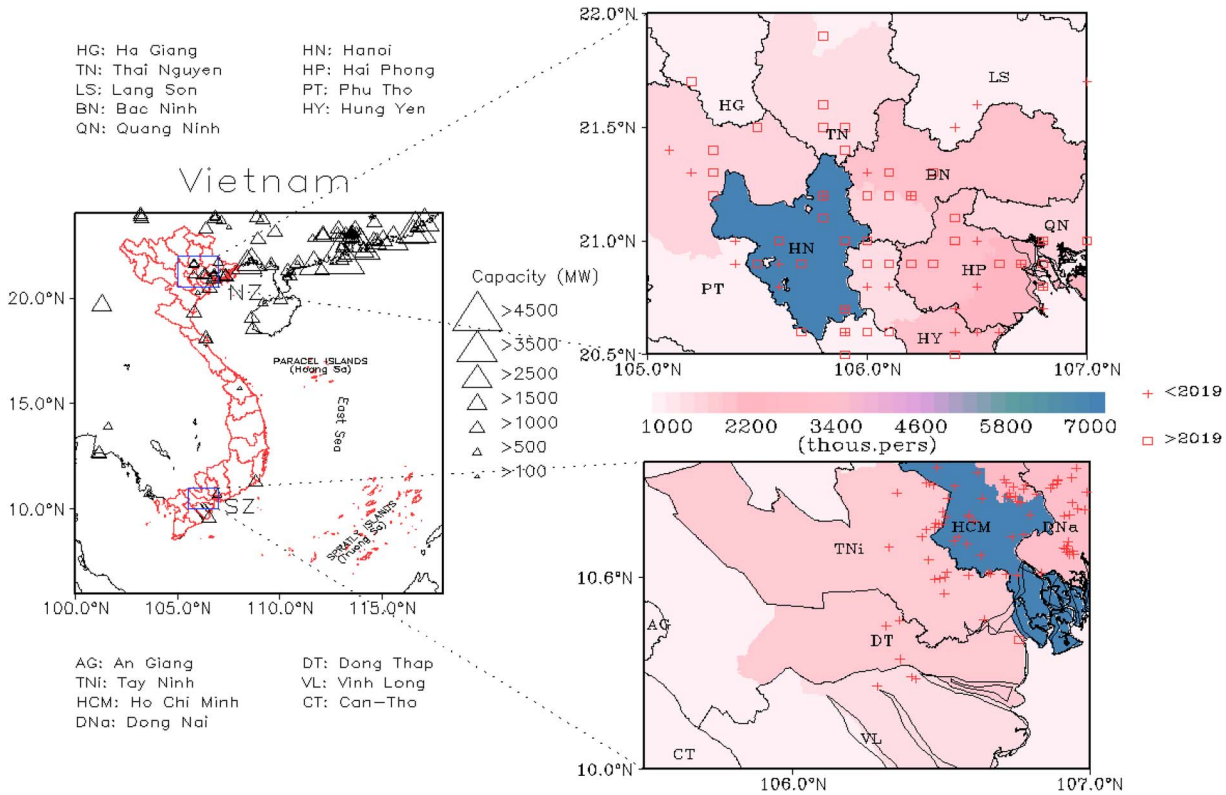

Fig. 1 Map of the study area – Population and distribution of industrial zones in the Northern (top) and Southern (bottom) regions. Triangles, rectangles, and plus symbols demonstrate….

spans from December to April of the following year. The Northern Zone experiences a subtropical climate with cold, dry winters favoring pollutant accumulation, while the Southern Zone has a tropical climate with distinct wet-dry seasons promoting dispersion during rains.

2.2. Data and model

2.2.1. MERRA2. Since 1980, MERRA-2 has been providing data. The dataset is generated using the Goddard Earth Observing System, Version 5 (GEOS-5) atmospheric model in combination with the data assimilation system, version 5.12.4.[15] The GEOS-5 model operates on a cubed-sphere grid with a native horizontal resolution of approximately 50 km and 72 hybrid-eta vertical layers, extending from the Earth's surface to 0.01 hPa.[3] With advancements in meteorological data assimilation, MERRA-2 represents a major advancement toward the comprehensive Earth System reanalysis framework currently being developed at the Global Modeling and Assimilation Office (GMAO).[16]

In this study, we use monthly MERRA-2 data downloaded *via* https://disc.gsfc.nasa.gov, including CO, SO_2, and BC. Aerosol components from the MERRA-2 reanalysis were incorporated to estimate $PM_{2.5}$ concentrations. This methodology has been extensively adopted in studies across different parts of the world, including Asia and Europe,[5–8] and has been employed in several recent MERRA-2-based investigations:

$$[PM_{2.5}] = 1.375 \times [SO_4^{2-}] + 1.8 \times [OC] + [BC] + [DU_{2.5}] + [SS_{2.5}] \quad (1)$$

[BC]: black carbon surface mass concentration, [$DU_{2.5}$]: dust surface mass concentration – $PM_{2.5}$, [OC]: organic carbon surface mass concentration, [SO_4^{2-}]: SO_4^{2-} surface mass concentration, [$SS_{2.5}$]: sea salt surface mass density – $PM_{2.5}$

2.2.2. Observational data for $PM_{2.5}$. The hourly $PM_{2.5}$ data used in this study were collected from automatic monitoring stations operated by the United States Environmental Protection Agency (EPA), located at the U.S. Embassy in Hanoi and the U.S. Consulate in Ho Chi Minh City. The $PM_{2.5}$ concentration data were downloaded from the official EPA website.[17] The data were processed to remove suspected or missing values prior to analysis.[11] The hourly data were averaged for monthly data and separated into seasons [winter (December–January–February), spring (March–May–April), summer (June–July–August), autumn (September–October–November) for the North; dry (December to April) and wet (May to November) for the South] in five year 2019–2023 period.

2.2.3. Statistical analyses. We applied the Spearman's correlation analysis to evaluate the relationship between monthly mean concentrations of $PM_{2.5}$ and other pollutants such as CO, SO_2, and BC. To ensure spatial consistency between ground observations and gridded data from MERRA-2, the model grid cell containing the corresponding monitoring site was used. The Spearman's correlation coefficient is a rank-

based measure of association between two variables, making it highly robust to non-linear relationships and outliers.[18] The mathematical formula for the Spearman correlation is as follows:

For two datasets $X = x_1, x_2,\ldots, x_n$ và $Y = y_1, y_2,\ldots, y_n$, the Spearman correlation coefficient (ρ) is determined by first converting each value into its corresponding rank $R(x_i)$ and $R(y_i)$, and then applying the following formula:

$$\rho = 1 - \frac{6\sum d_i^2}{n(n^2-1)} \quad (2)$$

Here, $d_i = R(x_i) - R(y_i)$ represents the difference in ranks for each observation pair, and n denotes the total number of samples. The statistical significance of the correlation coefficient (ρ) is evaluated using the Student's t-distribution, as expressed by the following formula:

$$t = \rho\sqrt{\frac{n-2}{1-\rho^2}} \quad (3)$$

where t follows a t-distribution with $n - 2$ degrees of freedom.

2.2.4. Backward trajectories and potential source contribution function. The HYSPLIT model[19] was used to identify potential source regions contributing to air pollution that affects air quality in HN and HCM. For the model setup, meteorological data were obtained from the National Centers for Environmental Prediction (NCEP) and the National Center for Atmospheric Research (NCAR) of National Oceanic and Atmospheric Administration (NOAA, USA); the backward trajectory duration was set to 72 hours; the starting altitude of the trajectories was 20 meters above ground level;[20] the time interval between trajectory points was 3 hours; and the receptor locations were set at HN (21.022 °N, 105.819 °E) and HCM (10.78 °N, 106.7 °E). In this study, backward trajectories were initialized at 20 m above ground level (AGL) to represent near-surface air masses directly relevant to human exposure and ground-based $PM_{2.5}$ observations. This approach is consistent with previous applications of HYSPLIT–PSCF methods for surface air pollution studies, where near-surface trajectories are commonly used to identify potential source regions influencing urban air quality.[21]

We acknowledge that trajectory height can significantly influence air mass pathways. Previous studies have shown that trajectories initialized at different altitudes may produce substantially different transport patterns due to vertical wind shear and atmospheric stratification. In addition, higher-altitude trajectories tend to represent regional-scale transport, whereas lower-altitude trajectories better capture near-surface pollutant transport processes.[22] The emission source areas of $PM_{2.5}$ on the non-local scale (*i.e.*, outside HN and HCM) can be identified using the PSCF model adopting the backward air trajectory, considering the heights, latitudes, and longitudes of trajectory segments. The PSCF values were computed following eqn (4):[22]

$$\mathrm{PSCF} = \frac{m_{ij}}{n_{ij}} \quad (4)$$

where m_{ij} is the number of trajectory endpoints falling within cell (i,j) and having $PM_{2.5}$ concentration higher than a threshold value (75th percentile), and n_{ij} denotes the total number of trajectory endpoints arriving at cell (i,j), and the weighting function to reduce the effects of low n_{ij}.

2.2.5. Fire detection counts. To identify hotspots, active fire data from the Terra and Aqua MODIS-C6 datasets (with a spatial resolution of 1 km × 1 km), provided by the Fire Information for Resource Management System (FIRMS; https://firms.eosdis.nasa.gov), were analyzed for the study area during the period from January 2019 to December 31, 2023. Detailed information on the algorithms and supporting products for MODIS fire detection can be found in Giglio *et al.*, (2003, 2016). To reduce uncertainty in the analysis, fire detections with low confidence (defined as confidence <50%) and ambiguous fire types (type ≠0) were excluded from the analysis.[23,24]

3. Results

3.1. Long-term trends and spatial distribution of pollutants assessed from MERRA-2

Regarding CO, this gas is a byproduct of incomplete combustion, where insufficient oxygen prevents carbon from fully converting to CO_2, leading instead to the formation of CO.[25] A significantly higher concentration is observed in the North (notably in Hanoi and its surrounding areas – marked in dark red, concentrated in the Red River Delta), extending along the Vietnam-China border; in contrast, the South exhibits lower concentrations, with moderate levels around Ho Chi Minh (Fig. 2a-1). A sharp spike in CO concentrations was recorded in 1998s, with levels in the South exceeding those in the North (Fig. 2b-1). This 1998 peak coincided with widespread biomass burning events in Southeast Asia, as evidenced by elevated fire activity during the El Niño year. This anomaly may be attributed to the influence of green industrial activities and the widespread practice of rice straw burning during that period (Faïn *et al.*, 2024). This finding is consistent with previous research on the impact of different emission sources across the Northern and Southern Hemisphere.[26] A pronounced high CO concentration was observed in Northern Vietnam, peaking during the 2015–2019 period, reflecting the significant impacts of urban traffic and residential combustion activities. This was followed by a sharp declined after that period, the reduction in CO concentrations in southern Vietnam was more gradual and exhibited less variability (Fig. 2b-1).

The northern Vietnam had a distinct seasonal pattern: CO levels peaked during December–January–February (DJF, winter) and reached their lowest during June–July–August (JJA, summer) (Fig. 2c-1), consistent with thermal inversion effects limiting vertical mixing.[27] Meanwhile, in the southern Vietnam, the results indicate higher concentrations from November to April (mainly in dry season) than from May to October (mainly in rainy season) (Fig. 2c-1).

Regarding SO_2, the long-term average (1980–2023) indicates a clear concentration in northeastern Vietnam (Fig. 2a-2). These areas also host a high density of industrial parks (Fig. 1), along

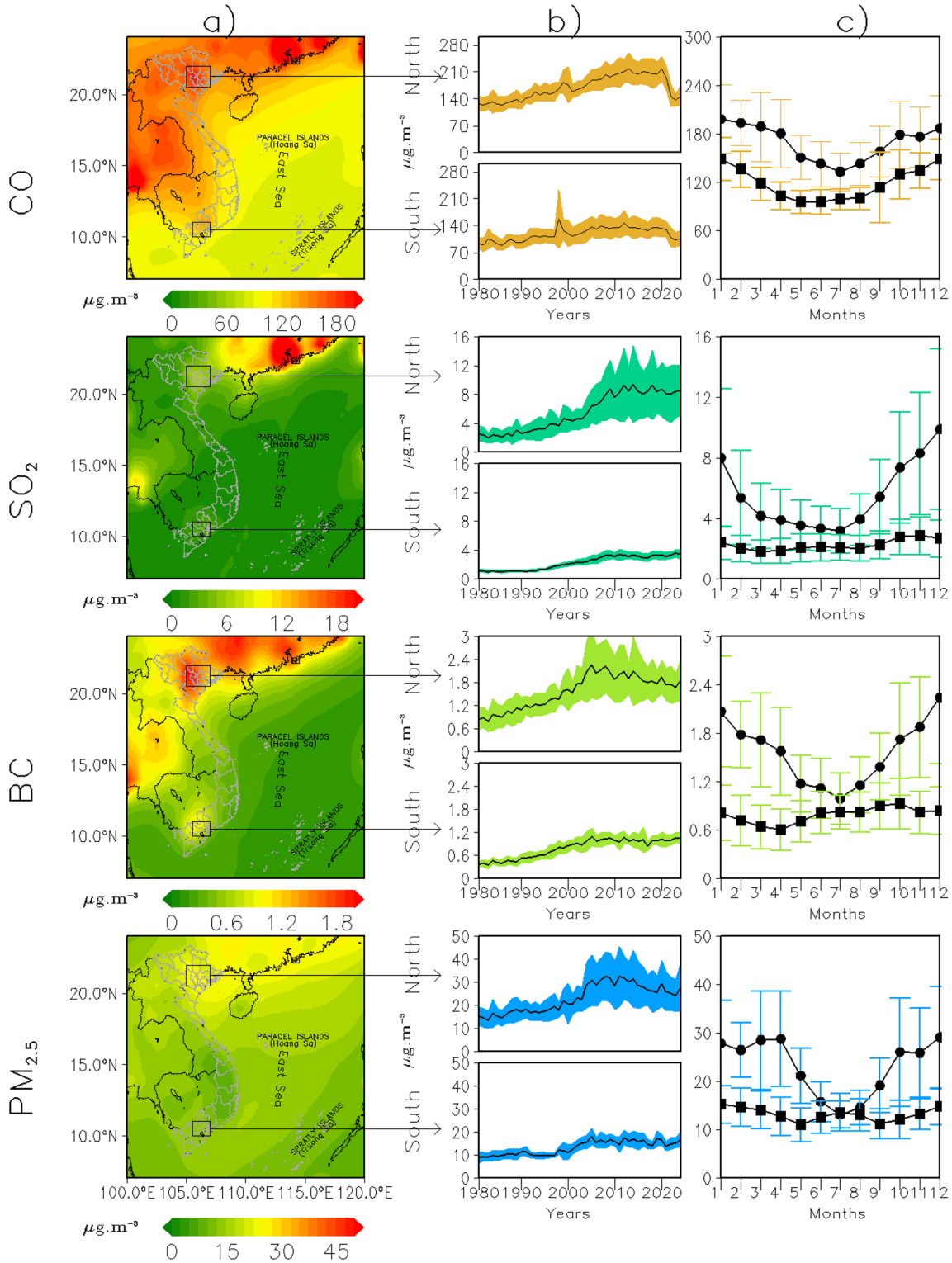

Fig. 2 (a) Average concentration of CO, SO_2, BC, and $PM_{2.5}$; (b) the interannual variations over northern and southern regions (monthly means with standard deviation); (c) the annual cycles by month, showing monthly means (filled circles: North; filled squared: South, with error bars representing standard deviation) over the period of 1980–2023.

with intense transportation and commercial activities – potential local emission sources of SO_2. Moreover, adjacent regions in southern China, considered the "world's factory" over the past two decades, exhibit markedly high SO_2 levels (shown in red), due to the intensive use of sulfur-rich fossil fuels in industrial sectors. Transboundary transport of pollutants from these regions likely contributes to elevated SO_2 concentrations over northern Vietnam. The interannual trend (Fig. 2b-2), showed

a gradual increase in SO_2 levels in the North until around 2010. This may be because of the controlling policy on coal-fired power plants in China, such as the 11th Five-Year Plan (2006–2010). In this period, the country aggressively eliminated outdated capacity, 76.83 GW compared to 50 GW as planned (Wang *et al.*, 2019, Cooperation, 2013). A subsequent slight decline aligns with the implementation of pollution control policies, particularly Vietnam's Prime Ministerial Directive 412/

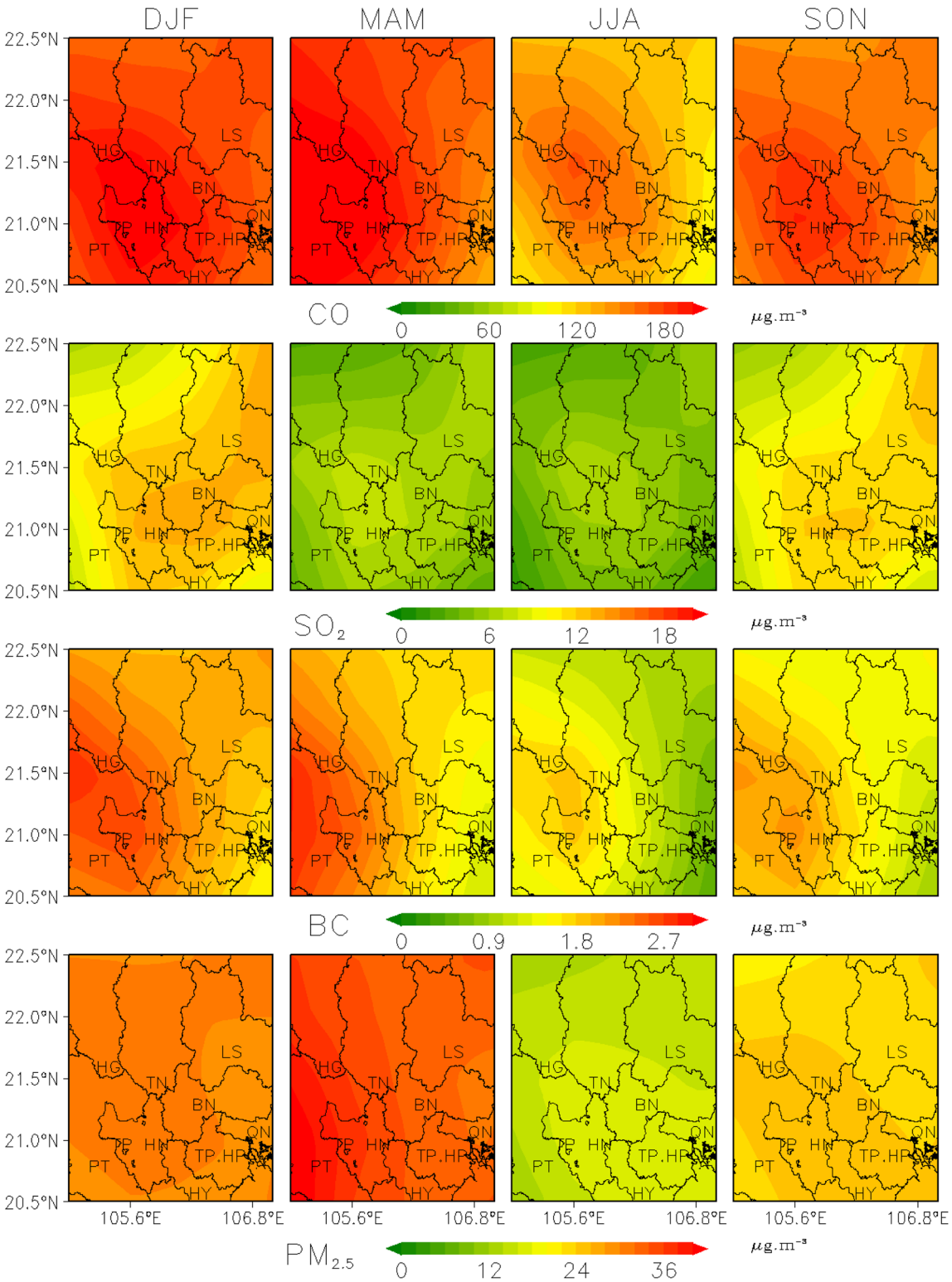

Fig. 3 Seasonal distributions of CO (row1), SO_2 (row2), BC (row3), and $PM_{2.5}$ (row 4) over northern Vietnam for the four seasons DJF (winter), MAM (spring), JJA (summer), and SON (autumn) during 2019–2023.

TTg-KTN, effective since 2015, which lowered the permissible sulfur content in diesel fuel from 0.25% to 0.05%. A related study on domestic shipping fuel likewise reports a 44% drop in SO_2 emissions following this policy shift (2015–2018).[28] In contrast, SO_2 in the South remained significantly lower and more stable throughout the observed period, at levels approximately four times lower than in the North (Fig. 2b-2). Seasonal variations in the North reveal a marked increase in SO_2 during winter-spring and a decrease during summer months (Fig. 2c-2). Meanwhile, the South maintained consistently lower SO_2 levels in all months (Fig. 2c-2). Recent deposition-based analyses confirm that monthly SO_2 fluctuations are more pronounced in the North than in the South – a pattern strongly influenced by meteorological variability and seasonality.[29] The finding supports our earlier results of a summertime minimum and wintertime peak (Fig. 2c-2).

Black carbon, formally defined as an ideally light-absorbing substance composed of carbon, is mostly formed in incomplete combustion of carbonaceous matter, namely wood, coal and fossil fuel.[30] The spatial distribution (Fig. 2a-3) clearly showed elevated BC concentration (1.2 to 1.8 μg m^{-3}, orange-red hues) over Northern Vietnam – spreading into southern China, whereas southern Vietnam exhibits substantially lower BC levels (<0.6 μg m^{-3}, green-light yellow), underscoring a marked north–south contrast. Both regions show a rising trend in BC from 1980 until around 2005–2010. Northern Vietnam exhibits a sharper increase, peaking during that period, followed by sustained high levels with a slight decline thereafter. Southern Vietnam also showed an upward trend but a lower magnitude and greater stability (Fig. 2b-3). Seasonal cycles are pronounced in the North: BC peaks during winter-spring (months 11, 12, 1, 2) with wider spread than the other months and reaches minimum in summer (months 6–8) (Fig. 2c-3). In contrast, the South experiences minimal seasonal fluctuation, with low and stable BC values year-round (Fig. 2c-3). Tran *et al.*, (2018) and Liu *et al.*, (2016) studies reported the negative correlation between BC and wind speed in Hanoi and Beijing, this imply the important role of meteorological parameters combined with topographical factor. Those studies also emphasize the positive correlation between BC and $PM_{2.5}$.

The highest concentrations of $PM_{2.5}$ are found in the Red River Delta region, extending into northern central Vietnam and Ho Chi Minh city (Fig. 2a-4), these areas strongly influenced by urbanization and industry.[31] Southern Vietnam exhibits significantly lower $PM_{2.5}$ levels, may reflecting fewer major emission sources and better ventilation conditions. From 2005 to 2019, northern Vietnam experienced a sharp rise in $PM_{2.5}$ concentrations, followed by marked decreases during COVID-19 lockdowns, and subsequent rebounds in 2022–2023 (Fig. 2b-4), align with recent findings.[10,32,33] Southern Vietnam displayed a more moderate and steady increase (Fig. 2b-4). Linear trend analysis showed an average increase of ~0.15 μg m^{-3} per year in the North from 2000–2019, compared to ~0.07 μg m^{-3} per year in the South (calculated *via* least-squares regression). Shape of seasonal variability of the Southern is different from the Northern. In this area, the peak $PM_{2.5}$ during the winter months (November to February), and lows in summer months (June, July, August) (Fig. 2c-4). Notably, northern Vietnam showed abrupt spikes in $PM_{2.5}$ during March–April, likely attributed to transboundary forest fires from Central southern Laos.[10,32] Meanwhile, southern Vietnam had stable monthly $PM_{2.5}$ concentration and smaller spread around monthly mean concentration in comparison with the northern (Fig. 2c-4).

In the following section, we focus on examining pollutant concentrations in the northern and southern regions of Vietnam over the most recent five-year period, from 2019–2023.

3.2. Seasonal variability of major pollutants in two regions

CO concentrations (row 1) peak sharply in DJF, exceeding ~185 ± 13 μg m^{-3} around Hanoi, Hung Yen, and Bac Ninh. Elevated CO levels (>135 μg m^{-3}) persist through spring (MAM) and autumn (SON), indicating a constant background pollution. This winter accumulation is attributable to frequent stagnant condition, compounded by fossil fuel burning (such as bee-hive stoves) in households and traffic emissions concentrated in heavily urban-industrial clusters.[32] SO_2 (row 2) reaches annual maxima in DJF (>12 μg m^{-3}) in industrial hubs such as Ninh Binh, Hai Phong – areas characterized by dense coal-fired power

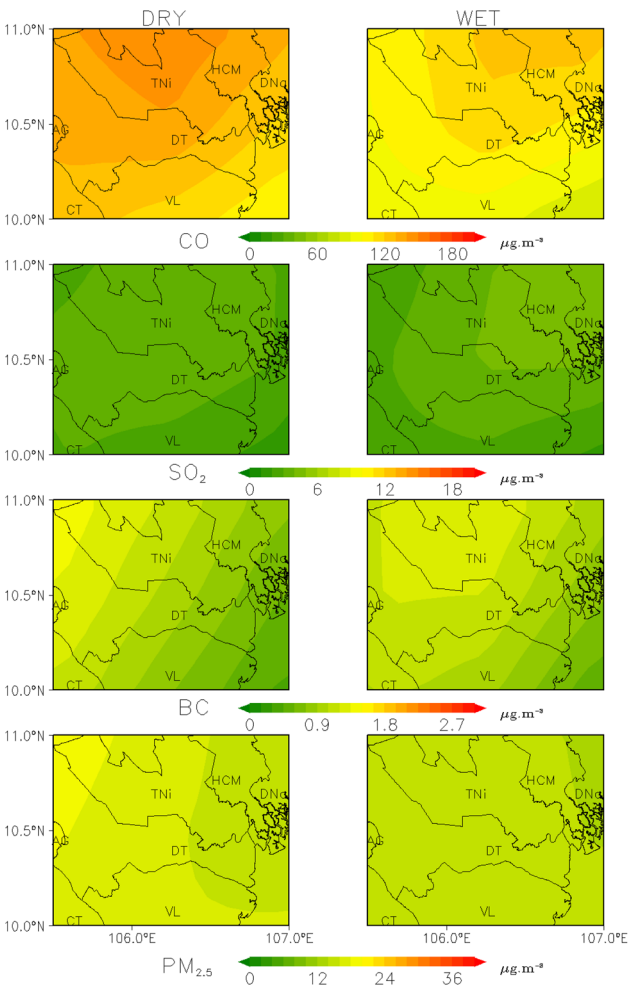

Fig. 4 Seasonal distributions of CO (row 1), SO_2 (row 2), BC (row 3), and $PM_{2.5}$ (row 4) over southern Vietnam for wet and dry seasons.

plants, cement, and steel factories.[32] Springtime (MAM) levels drop below 6 μg m^{-3}, particularly in peri-urban zone (Fig. 3). SO_2 hotspot patterns align with industrial point sources which is different with CO pattern, indicating different emission sources. BC (row 3) exhibits maximum value (>2.7 μg m^{-3}) during winter (DJF), particularly in the southwestern and central areas. BC decreased in spring (MAM) but remained moderately high, reaching lowest level in summer (JJA) and slightly increasing again in autumn (SON) (Fig. 3). $PM_{2.5}$ levels (row 4) are pronounced in DJF, exceeding 24 μg m^{-3} – well above WHO guideline of 5 μg m^{-3}. Spring spikes in $PM_{2.5}$, > 36 μg m^{-3} (Fig. 3) are likely associated with transboundary smoke from biomass fires in central southern Laos.[10,32]

CO levels in the dry season exceeded 150 μg m^{-3}, particularly in Ho Chi Minh City and Dong Nai, while in the wet season they drop significantly to below 120 μg m^{-3} (Fig. 4). This marked seasonal disparity underscores the meteorological influence. Dry-season conditions are typically associated with a shallower planetary boundary layer, weaker turbulence, and more frequent temperature inversions, leading to limited vertical mixing and higher accumulation of air pollutants. SO_2 remains low in both seasons (<6 μg m^{-3}) (Fig. 4) with no sharp contrast. Emission in southern Vietnam are less affected by coal-fired power plants and are thus far lower and less seasonally variable than in the North. Black carbon (BC) concentrations are modest, ranging from 0.6–1.2 μg m^{-3}. Areas close to the sea exhibited lower BC concentration compared to inland areas (Fig. 4). $PM_{2.5}$ in the dry season reached ~27 μg m^{-3} in urban and peri-urban zones, while in the wet season it declined to ~18 μg m^{-3}, still above the WHO guideline. Seasonality of $PM_{2.5}$ in HCM aligns with earlier findings where dry season peaks significantly exceed wet season values.[34]

The boxplots in Fig. 5 summarize grid-cell statistics: 5th, 25th, median (50th), 75th, and 95th percentiles), illustrating spatial dispersion of pollutant concentrations seasonally. CO exhibits a slight overall downward trend from 2019 to 2023, including the 95th percentile representing high-concentration grid-cells. This result supported other study in Hanoi where CO levels dropped by 28–41% during COVID-19 social distancing; even after weather normalization, CO remained 5–11% lower, indicating that reduced traffic volume was a primary driver of the decrease.[35] Wintertime (DJF) consistently recorded the highest median and upper percentiles, especially in 2019–2021, indicative of winter accumulation. In contrast, JJA maintained the lowest values, reflecting favorable dispersion and atmospheric cleansing during summer. Although levels decline over time, the length of the boxplots – particularly in 2019 and 2020 highlights pronounced spatial differences between densely and sparsely populated areas. This coincides with the COVID-19 lockdown period in northern Vietnam, during which industrial and transport activity was curtailed, but residential emissions (*e.g.*, cooking and domestic fuel use) may have increased. The observed CO reduction between 2019 and 2023 may partly reflect the implementation of the program to eliminate coal-fired "bee-hive" stoves – Decree 15/CT-UBND in Hanoi – to replace household coal heating (2017–2021). Alternatively, meteorological factors such as stronger winds could also have contributed. However, further targeted studies are required to firmly attribute causation. SO_2 showed clear seasonal variability but lacks of pronounced annual trend, this may be explained by the electricity demand driving coal-fired power plant activity in the region unchanged from 2019–2023. Winter (DJF) and autumn (SON) often exhibits slightly higher concentrations than spring (MAM) and summer (JJA) (Fig. 5), perhaps due to smaller capacity for dispersion. BC concentration peak in DJF and MAM, with median values ranging between 2.0–2.7 μg m^{-3}, the year 2023 with 75th percentile approaching 3.0 μg m^{-3}. JJA presents the lowest seasonal levels (median ~1.0–1.5 μg m^{-3}), with almost no value surpassing 2.0 μg m^{-3}. $PM_{2.5}$ concentration during DJF increased steadily post-2019. Spring (MAM) of 2023 showed a particularly high peak, similar to BC concentration peak in MAM-2023. JJA displayed narrower IQRs, indicating more homogeneous distribution attributable to rainfall and wind-driven dispersion.

Overall, SO_2 and BC show different seasonal behaviors compared to $PM_{2.5}$ and CO (Fig. 6). Dry-season CO levels were markedly higher than wet-season values, with differences ranging from ~30–50 μg m^{-3}, general declining trend is evident from 2019 through 2022, followed by a slight increase in 2023 (Fig. 6). SO_2 remained relatively low throughout the study period, typically within a range of ~5–8 μg m^{-3}, and exhibited no significant interannual spikes or seasonal difference (Fig. 6). However, the IQRs of wet seasons were longer than those of dry seasons. BC of two seasons exhibited no significant difference. However, opposite to SO_2, IQRs of BC in wet seasons were

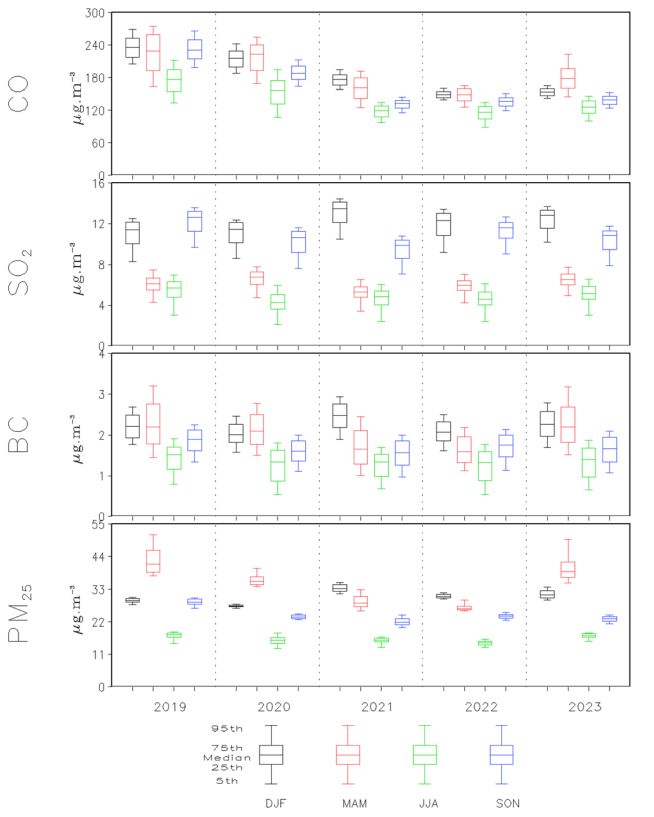

Fig. 5 Seasonal boxplots across northern Vietnam from 2019 to 2023.

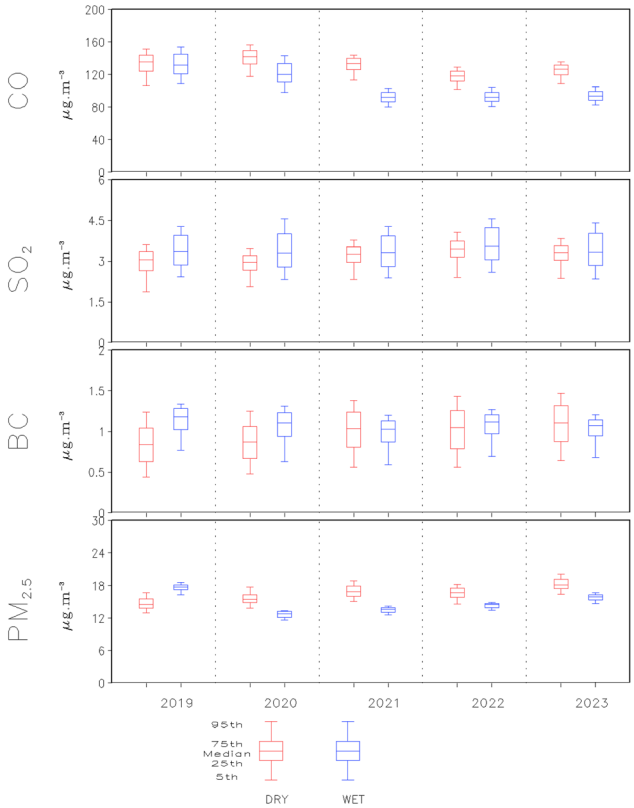

Fig. 6 Seasonal boxplots across southern Vietnam from 2019 to 2023.

shorter than those in dry seasons (Fig. 6). Except 2019, dry-season $PM_{2.5}$ levels are higher than wet-season levels in all years (Fig. 6). The IQRs of $PM_{2.5}$ are very short compared to those of other pollutants, indicating more uniform spatial distribution.

3.3. Identifying the influence of local and remote sources through the correlation between CO, SO_2, BC and $PM_{2.5}$ in two regions

Fig. 1 presents the time series of CO, SO_2, BC, and $PM_{2.5}$, revealing pronounced differences in both concentration levels and seasonal variability between the northern and southern regions. Overall, pollutant concentrations are consistently higher in the North than in the South, with particularly strong seasonal variations observed for SO_2, BC, and $PM_{2.5}$. In contrast, pollutant levels in the South exhibit relatively weaker seasonal variability. These regional differences can be attributed to a combination of emission sources and meteorological conditions. Both regions are metropolitan urban areas with substantial local emissions from transportation and industrial activities. For example, the North is surrounded by a larger number of coal-fired power plants compared to the South (Fig. 1),[11] whereas the South hosts a greater number of older industrial parks (Fig. 1 and Tables S1–S2). In addition, both regions may be influenced by biomass burning, originating not only from local sources but also from transboundary transport.[10,32,36] Meteorological factors further modulate these patterns (Fig. S2). The North experiences four distinct seasons, with low temperatures and reduced planetary boundary layer heights during winter, which suppress atmospheric mixing and dilution. Conversely, persistently high temperatures in the South promote a higher boundary layer throughout the year, enhancing pollutant dispersion. Wind patterns also play a critical role. In winter, prevailing northeasterly winds may transport air pollutants to the North, leading to elevated SO_2 concentrations. In contrast, the South is influenced by stronger marine winds that transport moist air masses, resulting in lower and less variable SO_2 levels. These findings are consistent with the conclusions reported by (ref. 11).

From Fig. 7, in Northern Vietnam, CO exhibited no correlation with $PM_{2.5}$ during the winter (DJF). This supports the hypothesis that wintertime $PM_{2.5}$ originates from various sources that do not coincide with CO, such as: long-range transport, rice straw burning, secondary organic aerosols. In contrast, BC showed a strong and consistent correlation with $PM_{2.5}$ throughout the year, especially during DJF, likely due to favorable meteorological conditions for accumulation of BC emissions from biomass and fossil fuel combustion. SO_2 displayed high correlations in DJF, MAM, and SON but no correlation in JJA, indicating that increased atmospheric mixing and ventilation during summer reduce its influence on $PM_{2.5}$. In Southern Vietnam, only BC showed a clear correlation with $PM_{2.5}$ during dry season, emphasizing the role of domestic fuel burning and small-scale industrial activities. All other pollutant showed no correlation with $PM_{2.5}$ (as shown in Fig. 7), suggesting that $PM_{2.5}$ formation in this region is influenced by other processes or more diffuse sources.

3.4. Seasonal correlation between MERRA-2-$PM_{2.5}$ and observed $PM_{2.5}$ in Hanoi and Ho Chi Minh

Spearman's correlation was employed to assess the monotonic relationship between modeled and observed $PM_{2.5}$ concentrations. In Hanoi, correlation coefficients were high and statistically significant during all four seasons, with the highest correlation observed in spring (MAM) (Fig. 8). Visually, the seasonal variation and absolute values of $PM_{2.5}$ from MERRA-2 closely resemble the observed data, as shown in Fig. 8. However, during winter (DJF), MERRA2 tends to underestimate $PM_{2.5}$ more significantly compared to observed value (Fig. 8). Despite this bias, MERRA-2 successfully captures the seasonal trends and dispersion patterns in Hanoi (Fig. 8). In Ho Chi Minh city, although MERRA2-$PM_{2.5}$ levels during the wet season are relatively close to observational data, MERRA2 generally failed to reproduce the seasonal contrasts between dry and wet seasons, as evident from low and statistically non-significant Spearman correlation values (Fig. 8). Moreover, MERRA2 significantly underestimate $PM_{2.5}$ during the dry season (Fig. 8). This systematic underestimation of $PM_{2.5}$ by MERRA2 has been consistently reported in various validation studies.[7,8,37,38] The underestimation in Hanoi's winter and HCMC's dry season may stem from MERRA-2's coarse resolution missing local urban emissions or inaccurate aerosol hygroscopicity in humid conditions. Moreover, these results are currently based on only

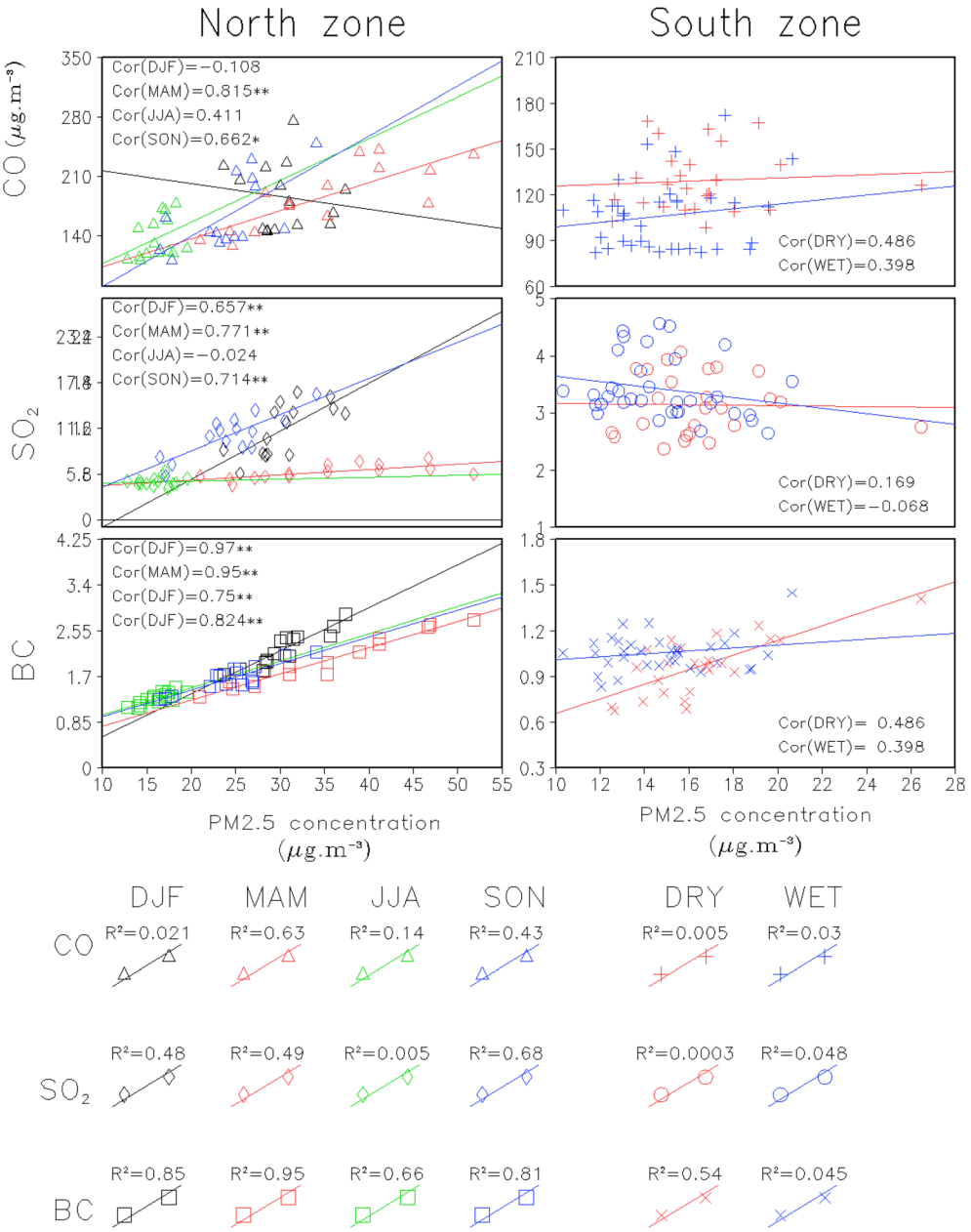

Fig. 7 Seasonal correlation between pollutants CO, SO_2, BC and $PM_{2.5}$ in Northern and Southern Vietnam.

two monitoring stations representing the northern and southern regions, selected due to their long-term and reliable data availability. Future research should include more comprehensive evaluations involving additional monitoring sites to enhance spatial representativeness and robustness.

3.5. Source identification of non-local sources *via* PSCF analysis

During DJF, the PSCF distribution covers South–Eastern China and along the East China coast (Fig. 9). This pattern highlights the dominant role of the northeast monsoon and cold surges in transporting polluted air masses from continental China to northern Vietnam during high-pollution episodes. These results are consistent with previous studies on wintertime long-range transport to Hanoi.[39,40] In addition, relatively high PSCF values are also observed over northern central Laos. In MAM, the PSCF extends over a broad area, shifting toward the west–northwest, with pronounced signals over northern Thailand, northern Laos, eastern Myanmar, and parts of Cambodia (Fig. 9). This coincides with the regional-scale biomass burning season in the upper Mekong subregion (February–April). Such findings suggest a substantial contribution from forest fires and shifting cultivation to elevated $PM_{2.5}$ episodes in Hanoi during the late dry season and the transition period.[41,42] In JJA, the PSCF values decrease markedly over the Indochina Peninsula, with only some remote signals appearing in northern China

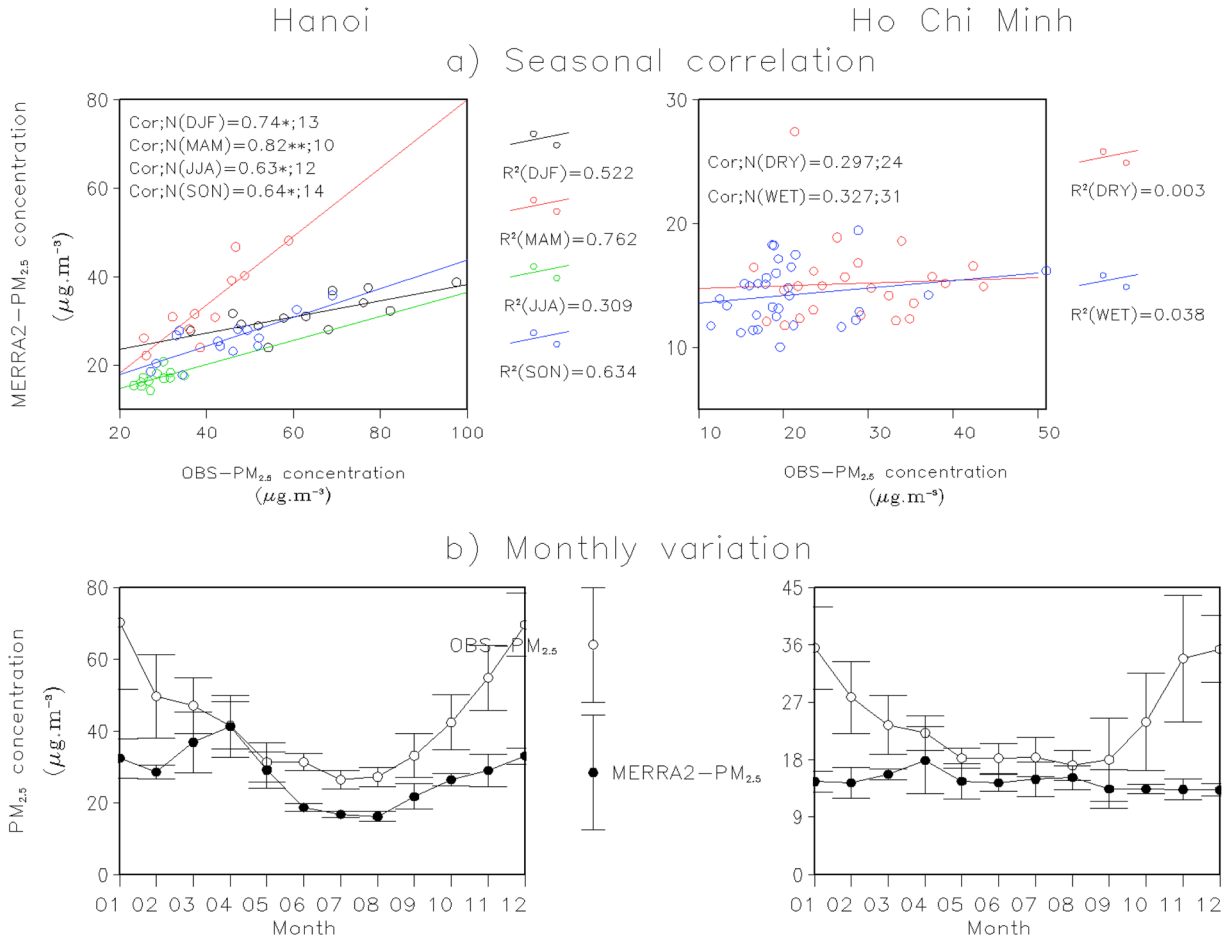

Fig. 8 (a) Seasonal correlation between MERRA-2-$PM_{2.5}$ and (b) Monthly variation of observed $PM_{2.5}$ in Hanoi and Ho Chi Minh City over the study period. Error bars represent standard deviation.

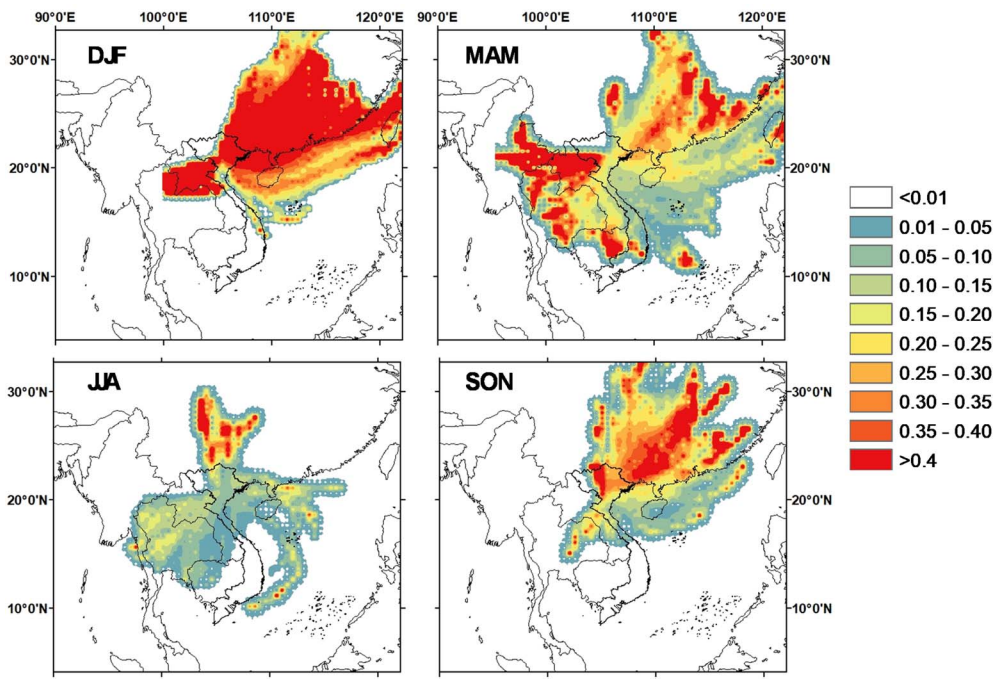

Fig. 9 PSCF maps using the threshold criteria of 50 μg m^{-3} for $PM_{2.5}$ from three-day backward air trajectories arriving in Hanoi.

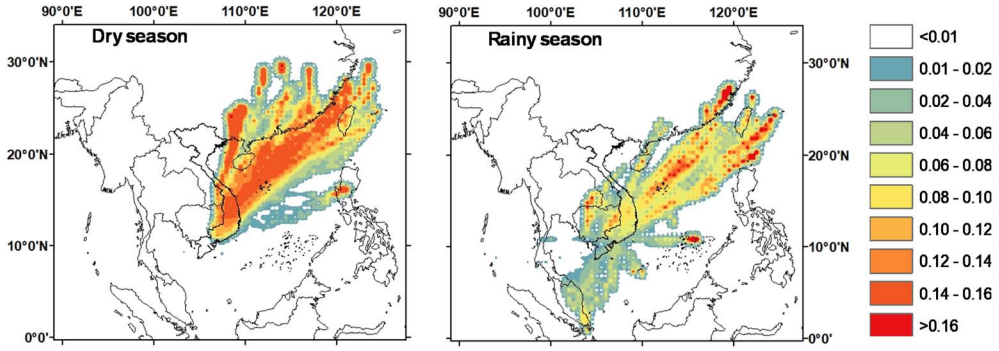

Fig. 10 PSCF maps using the threshold criteria of 50 μg m^{-3} for $PM_{2.5}$ from three-day backward air trajectories arriving in Ho Chi Minh.

(Fig. 9). This reduction is attributable to the southwest monsoon, which brings cleaner maritime air masses and heavy rainfall that enhances wet scavenging, thereby lowering the probability of external source contributions to high $PM_{2.5}$ levels. In SON, the PSCF signals intensify again over southeastern China and along the western coast of the South China Sea (Fig. 9), reflecting the re-establishment of the early northeast monsoon circulation.

In summary, for Hanoi, long-range transport from China dominates during the winter–autumn period, whereas biomass burning in the Mekong subregion plays a critical role in the late dry to early spring season. In contrast, the summer is characterized by weaker external influences due to precipitation and marine/sea-borne air masses.

During the dry season, a strong PSCF band extends in a southwest–northeast direction across the South China Sea

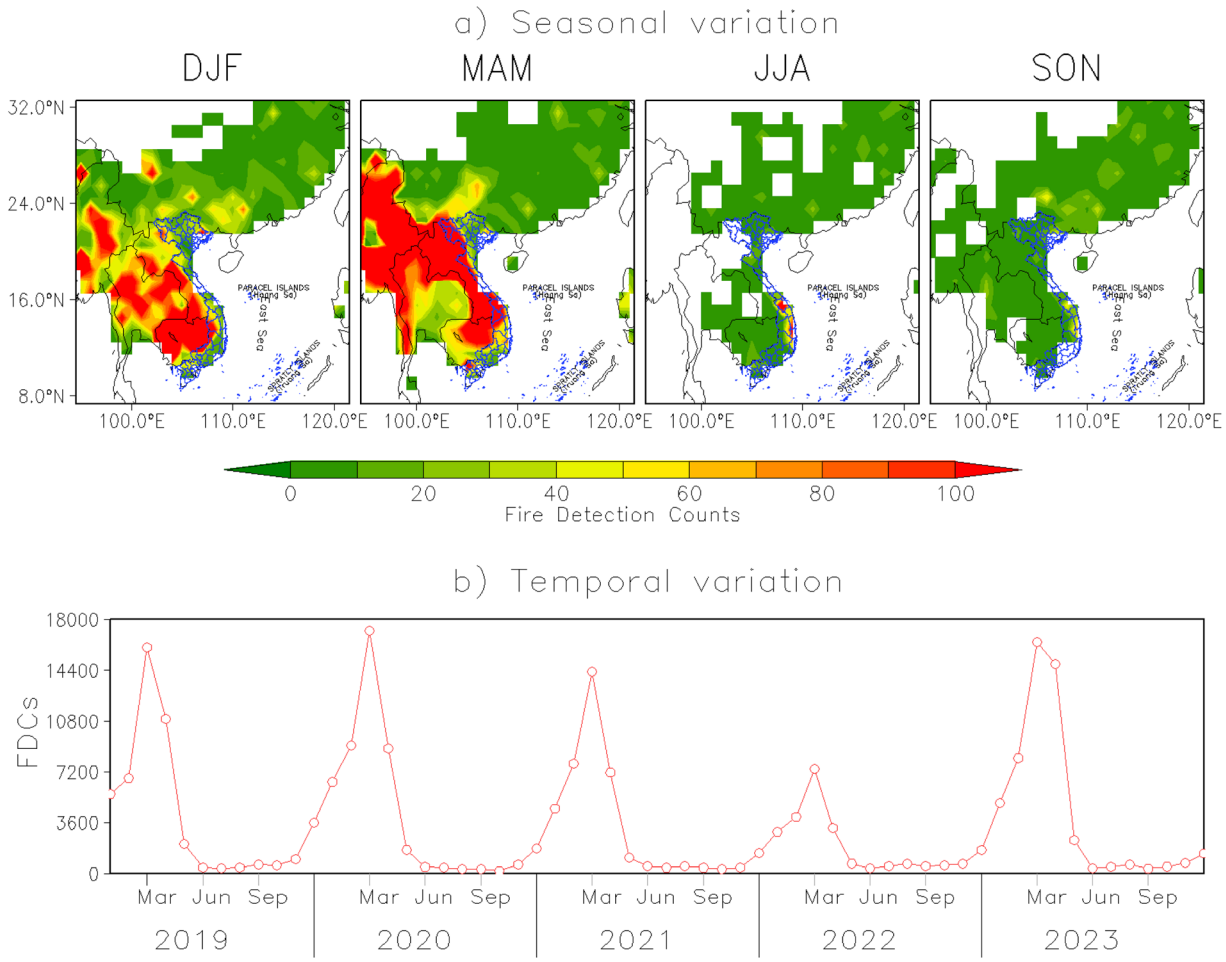

Fig. 11 (a) Seasonal distribution of fire hotspots over the PSCF domain influencing Hanoi; (b) temporal variation of fire detection counts (FDCs) from 2019 to 2023, highlighting peak biomass burning periods.

toward the Taiwan–Luzon region, while high values are also observed over the Southeastern region of Vietnam (Binh Duong, Dong Nai), where numerous industrial zones are concentrated (Fig. 10). This spatial pattern indicates two notable non-local source clusters contributing to high $PM_{2.5}$ episodes: (i) the South China Sea/shipping routes, likely associated with ship emissions transported by the northeast monsoon, and (ii) the industrial belt of Southeastern Vietnam. These findings are consistent with the results of T. N. T. Nguyen *et al.*, (2023), who identified the South China Sea and Southeastern Vietnam as important non-local source regions for Ho Chi Minh City during the dry season.[43]

In the wet season, the PSCF intensity decreases across southern Vietnam (Fig. 10) due to heavy rainfall and high precipitation frequency, which enhances wet deposition. Nevertheless, elongated PSCF "stripes" remain along the northeast corridor across the South China Sea, together with a cluster over the Mekong Delta. This suggests a potential contribution from post-harvest biomass residue burning during the Summer–Autumn crop; however, the influence is substantially weakened by precipitation. Overall, the role of non-local sources is relatively minor compared to local emissions (traffic and residential activities) during the wet season[43]

3.6. Fire detection counts

In practice, biomass burning contributes up to 40% of global carbon emissions.[44] Therefore, the detection of fire hotspots by satellite can be used to assess the impact of forest and biomass burning on $PM_{2.5}$ concentrations at specific locations. Therefore, the FDCs covering above PSCF domains was investigated and displayed in Fig. 11 for North zone and in Fig. 12 for South zone.

In spring (MAM), the highest density of fire hotspots is observed, with strong concentrations over northern Thailand, Laos, and parts of Cambodia (Fig. 11a). This is consistent with the springtime PSCF results for Hanoi (Fig. 9), where potential source regions extend west–northwestward, indicating that biomass burning in the Mekong subregion is a key contributor to elevated $PM_{2.5}$ episodes in Hanoi. In winter (DJF), fire activity is also recorded but at moderate levels, whereas in summer (JJA)

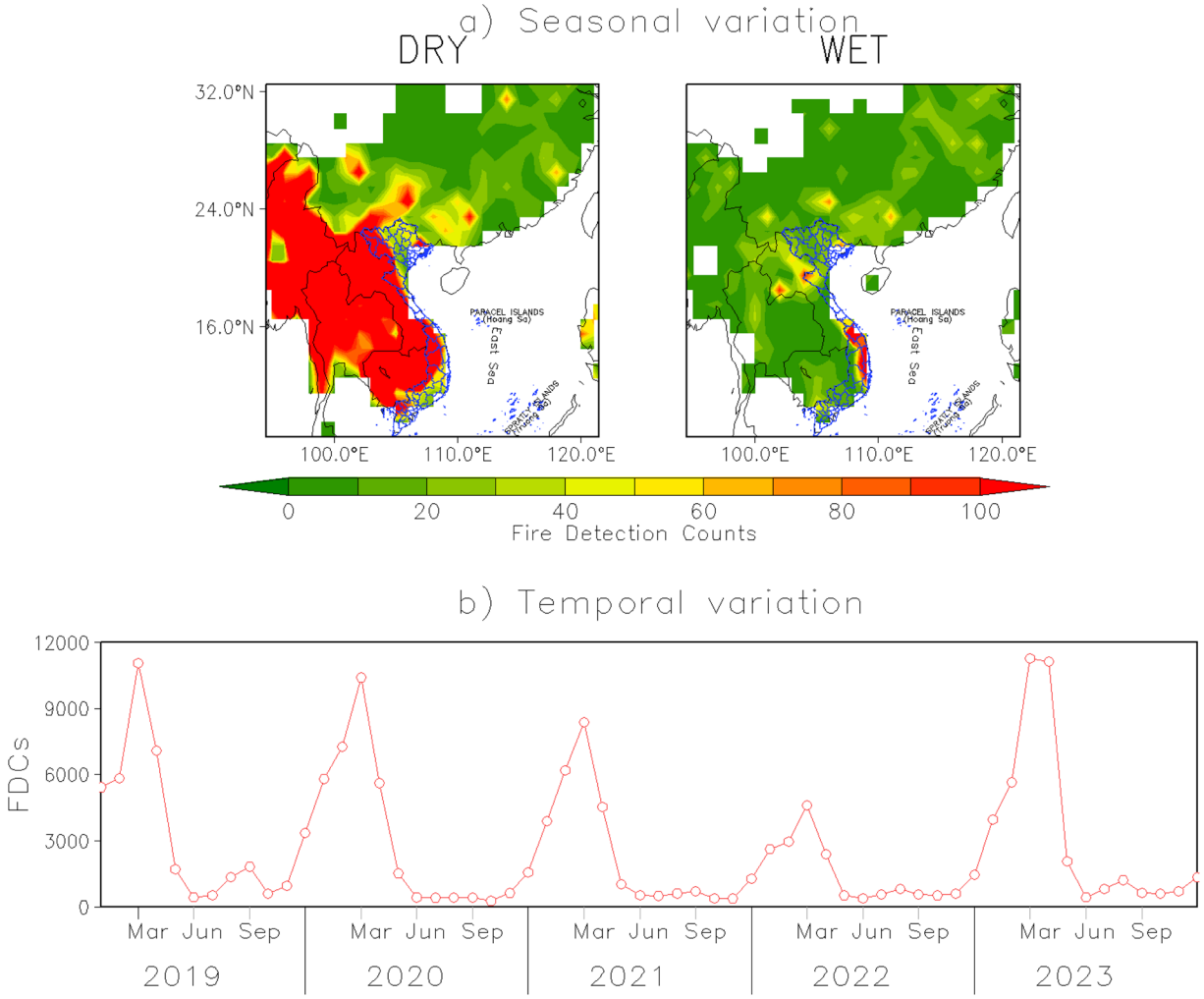

Fig. 12 (a) Seasonal distribution of fire hotspots over the PSCF domain influencing Ho Chi Minh City; (b) temporal variation of fire detection counts (FDCs) from 2019 to 2023.

and autumn (SON) it is nearly negligible, consistent with the PSCF results showing very limited external source contributions during summer. The temporal variation during 2019–2023 reveals pronounced peaks of FDCs occurring regularly between February and April each year (Fig. 11b). The coincidence between these FDC maxima and the PSCF high-probability regions confirms that biomass smoke originating from northwestern areas and the Mekong subregion is a major transboundary source contributing to $PM_{2.5}$ pollution in Hanoi during MAM.

During the dry season, fire hotspots are densely concentrated in Cambodia, southern Laos, eastern Thailand, and the Mekong Delta (Fig. 12). This coincides with the PSCF results for Ho Chi Minh City (Fig. 10), which show high probabilities extending from the west–northwest (Cambodia, Laos) as well as local contributions from the Southeastern region of Vietnam. These patterns suggest that rice-residue burning and forest fires in the lower Mekong region may contribute to elevated $PM_{2.5}$ levels in Ho Chi Minh City during the dry season. In contrast, almost no significant fire activity is observed in the wet season, which is consistent with the weak PSCF signals for Ho Chi Minh City during this period, largely due to heavy rainfall and enhanced wet deposition. The temporal variation (2019–2023) in Fig. 12b shows recurring peaks between February and April, although with much lower intensity compared to northern Vietnam. This implies that biomass burning still plays a role in $PM_{2.5}$ pollution in Ho Chi Minh City, but its influence is less pronounced than in Hanoi, as Ho Chi Minh City is more strongly affected by industrial and shipping emissions.

4. Conclusion

This study provides the first long-term (1980–2023) spatiotemporal assessment of CO, SO_2, BC, and $PM_{2.5}$ across Vietnam's two largest urban–industrial regions. By integrating MERRA2 reanalysis with ground-based validation, correlation analysis, and PSCF modeling, we identified both local and long-range drivers of air pollution.

Pollutant concentrations were consistently higher in the North, shaped by dense industry, meteorological conditions, and cross-border transport from neighboring countries. Seasonal analysis revealed pronounced winter peaks in the North linked to stagnant meteorology, while the South exhibited weaker seasonal variability. Among pollutants, black carbon showed the strongest correlation with $PM_{2.5}$, highlighting its central role in fine particle composition.

MERRA2 successfully reproduced seasonal $PM_{2.5}$ patterns but underestimated absolute concentrations, especially in Ho Chi Minh City during the dry season, underscoring the importance of an expanded monitoring network. PSCF results identified biomass burning as a major external contributor to Hanoi (springtime fires in the Mekong subregion), whereas in Ho Chi Minh City its influence was secondary to dominant local sources such as traffic, industry, and shipping.

This work advances the understanding of Vietnam's air quality by disentangling local and transboundary influences. The methodology offers a framework for future research as monitoring networks expand. Incorporating additional reanalysis products (*e.g.*, CAMS, TCR), higher-resolution fire datasets (*e.g.*, VIIRS), and broader pollutant validation will enhance source attribution and better support evidence-based air quality management aligned with Vietnam's net-zero targets.

Conflicts of interest

There are no conflicts to declare.

Data availability

The datasets generated and/or analyzed during the current study are available from the corresponding author on reasonable request.

Supplementary information (SI) is available. See DOI: https://doi.org/10.1039/d5va00367a.

Acknowledgements

Funding This research was funded by the National Foundation for Science and Technology Development (Nafosted) under grant number 104.04–2020.20.

References

1 A. Inness, M. Ades, A. Agustí-Panareda, J. Barré, A. Benedictow, A. M. Blechschmidt, J. J. Dominguez, R. Engelen, H. Eskes, J. Flemming, V. Huijnen, L. Jones, Z. Kipling, S. Massart, M. Parrington, V. H. Peuch, M. Razinger, S. Remy, M. Schulz and M. Suttie, *Atmos. Chem. Phys.*, 2019, **19**, 3515–3556.
2 K. Miyazaki, H. J. Eskes, K. Sudo, M. Takigawa, M. van Weele and K. F. Boersma, *Atmos. Chem. Phys.*, 2012, **12**, 9545–9579.
3 C. A. Randles, A. M. da Silva, V. Buchard, P. R. Colarco, A. Darmenov, R. Govindaraju, A. Smirnov, B. Holben, R. Ferrare, J. Hair, Y. Shinozuka and C. J. Flynn, *J. Clim.*, 2017, **30**, 6823–6850.
4 W. A. Lahoz and P. Schneider, *Front. Environ. Sci.*, 2014, **2**, 2014.
5 G. Tuna Tuygun, S. Gündoğdu and T. Elbir, *Air Qual. Atmos. Health*, 2022, **15**, 2283–2297.
6 F. Borhani, A. H. Ehsani, M. Shafiepour Motlagh and Y. Rashidi, *Environ. Dev. Sustain.*, 2024, **26**, 5775–5816.
7 C. D. Navinya, V. Vinoj and S. K. Pandey, *Aerosol Air Qual. Res.*, 2020, **20**, 1329–1339.
8 R. Sinha, P. Madan, R. Singh and L. Gupta, *E3S Web of Conferences*, 2024, vol. 559, p. 01005.
9 K. Lasko, K. P. Vadrevu and T. T. N. Nguyen, *PLoS One*, 2018, **13**, e0196629.
10 T.-H. Nguyen, Q.-T. Phan, H.-T. Van and D.-A. Dam, *Water, Air, Soil Pollut.*, 2025, **236**, 401.
11 Q. T. Vuong, P. Q. Thang and L. V. Linh, *Environ. Monit. Assess.*, 2025, **197**, 1322.
12 WHO global air quality guidelines: particulate matter ($PM_{2.5}$ and PM_{10}), ozone, nitrogen dioxide, sulfur dioxide and carbon monoxide, accessed 25 July 2025.

13 The Paris Agreement, https://unfccc.int/process-and-meetings/the-paris-agreement, accessed 25 July 2025.
14 ASEAN Declaration on Environmental Sustainability, accessed 25 July 2025.
15 L. T. Andrea Molod, M. Suarez, J. Bacmeister, S. In-Sun and A. Eichmann, *The GEOS-5 Atmospheric General Circulation Model: Mean Climate and Development from MERRA to Fortuna*, Goddard Space Flight Center, 2012, https://ntrs.nasa.gov/api/citations/20120011790/downloads/20120011790.pdf.
16 R. Gelaro, W. McCarty, M. J. Suárez, R. Todling, A. Molod, L. Takacs, C. A. Randles, A. Darmenov, M. G. Bosilovich, R. Reichle, K. Wargan, L. Coy, R. Cullather, C. Draper, S. Akella, V. Buchard, A. Conaty, A. M. da Silva, W. Gu, G.-K. Kim, R. Koster, R. Lucchesi, D. Merkova, J. E. Nielsen, G. Partyka, S. Pawson, W. Putman, M. Rienecker, S. D. Schubert, M. Sienkiewicz and B. Zhao, *J. Clim.*, 2017, **30**, 5419–5454.
17 Air quality data, https://www.airnow.gov, accessed 25 Jul 2025.
18 H. Akoglu, *Turk. J. Emerg. Med.*, 2018, **18**, 91–93.
19 A. F. Stein, R. R. Draxler, G. D. Rolph, B. J. B. Stunder, M. D. Cohen and F. Ngan, *Bull. Am. Meteorol. Soc.*, 2015, **96**, 2059–2077.
20 B.-T. Ly, Y. Matsumi, T. V. Vu, K. Sekiguchi, T.-T. Nguyen, C.-T. Pham, T.-D. Nghiem, I.-H. Ngo, Y. Kurotsuchi, T.-H. Nguyen and T. Nakayama, *J. Aerosol Sci.*, 2021, **152**, 105716.
21 P. K. Hopke, *J. Air Waste Manage. Assoc.*, 2016, **66**, 237–259.
22 Y.-K. Hsu, T. M. Holsen and P. K. Hopke, *Atmos. Environ.*, 2003, **37**, 545–562.
23 L. Giglio, J. Descloitres, C. O. Justice and Y. J. Kaufman, *Rem. Sens. Environ.*, 2003, **87**, 273–282.
24 L. Giglio, W. Schroeder and C. O. Justice, *Rem. Sens. Environ.*, 2016, **178**, 31–41.
25 C. Deheri, S. K. Acharya, D. N. Thatoi and A. P. Mohanty, *Fuel*, 2020, **260**, 116337.
26 X. Faïn, S. Szopa, V. Naïk, P. Martinerie, D. M. Etheridge, R. H. Rhodes, C. M. Trudinger, V. V. Petrenko, K. Fourteau and P. Place, *Preindustrial to present-day changes in atmospheric carbon monoxide: agreements and gaps between ice archives and global model reconstructions*, EGUsphere, 2024, vol. 2024, pp. 1–23, DOI: 10.5194/egusphere-2024-653.
27 T. T. Trinh, T. T. Trinh, T. T. Le, T. D. H. Nguyen and B. M. Tu, *Environ. Geochem. Health*, 2019, **41**, 929–937.
28 T. T. Huyen, N. T. K. Oanh, L. N. Huy, E. Winijkul and N. N. H. Chi, *Environ. Technol. Innov.*, 2022, **27**, 102507.
29 M. T. Nguyen, *IgMin Research In*, 2024.
30 A. Petzold, J. A. Ogren, M. Fiebig, P. Laj, S. M. Li, U. Baltensperger, T. Holzer-Popp, S. Kinne, G. Pappalardo, N. Sugimoto, C. Wehrli, A. Wiedensohler and X. Y. Zhang, *Atmos. Chem. Phys.*, 2013, **13**, 8365–8379.
31 T. Nhat Thanh Nguyen, H. Anh Le, T. Minh Tra Mac, T. Trang Nhung Nguyen, V. Ha Pham and Q. Hung Bui, *Glob. Environ. Res.*, 2018, **22**, 73–83.
32 Q. T. Bui, D. L. Nguyen and T. H. Bui, *Atmosphere*, 2022, **13**, 1911.
33 G. T. H. Nguyen, H. Hoang-Cong and L. T. La, *Water, Air, Soil Pollut.*, 2023, **234**, 85.
34 T. T. Hien, N. D. T. Chi, N. T. Nguyen, L. X. Vinh, N. Takenaka and D. H. Huy, *Aerosol Air Qual. Res.*, 2019, **19**, 2239–2251.
35 N. H. Le, B.-T. Ly, P. K. Thai, G.-H. Pham, I.-H. Ngo, V.-N. Do, T. T. Le, L. V. Nhu, H. D. Son, Y.-L. T. Nguyen, D. H. Pham and T. V. Vu, *Aerosol Air Qual. Res.*, 2021, **21**, 210081.
36 N. Tran, Y. Fujii, V. X. Le, D. T. C. Nguyen, H. Okochi, T. Thi Hien and N. Takenaka, *Aerosol Air Qual. Res.*, 2023, **23**, 220312.
37 A. Dhandapani, J. Iqbal and R. N. Kumar, *Chemosphere*, 2023, **340**, 139966.
38 J. Ma, J. Xu and Y. Qu, *Atmos. Environ.*, 2020, **237**, 117666.
39 B. A. Phung Ngoc, H. Delbarre, K. Deboudt, E. Dieudonné, D. Nguyen Tran, S. Le Thanh, J. Pelon and F. Ravetta, *Atmos. Pollut. Res.*, 2021, **12**, 101068.
40 B.-A. Phung-Ngoc, E. Dieudonné, H. Delbarre, K. Deboudt, S.-T. Nguyen, V.-H. Bui, D.-M. Vu and H.-T. Nguyen-Thi, *Atmos. Environ.*, 2023, **300**, 119669.
41 T. Amnuaylojaroen and N. Parasin, *Toxics*, 2023, **11**, 553.
42 N. D. Luong, N. Chuersuwan, H. T. Viet and B. Q. Trung, *APN Sci. Bull.*, 2022, **12**(1), 56–65.
43 T. N. T. Nguyen, N. X. Du and N. T. Hoa, *Atmosphere*, 2023, **14**, 579.
44 V. Ramanathan and G. Carmichael, *Nat. Geosci.*, 2008, **1**, 221–227.